SCIENTIFIC REPORTS

OPEN

SUBJECT AREAS:
DRUG DELIVERY
ORGANIC-INORGANIC NANOSTRUCTURES

Received
12 October 2014

Accepted
16 December 2014

Published
19 January 2015

Correspondence and requests for materials should be addressed to J.L. (jlin@ciac.ac.cn) or Z.Y.H. (zyhou@ciac.ac.cn)

Aptamer-Mediated Up-conversion Core/MOF Shell Nanocomposites for Targeted Drug Delivery and Cell Imaging

Kerong Deng[1,2], Zhiyao Hou[1], Xuejiao Li[1], Chunxia Li[1], Yuanxin Zhang[1], Xiaoran Deng[1,2], Ziyong Cheng[1] & Jun Lin[1]

[1]State Key Laboratory of Rare Earth Resource Utilization, Changchun Institute of Applied Chemistry, Chinese Academy of Sciences, Changchun 130022, P. R. China, [2]University of Chinese Academy of Sciences, Beijing 100049, P. R. China.

Multifunctional nanocarriers for targeted bioimaging and drug delivery have attracted much attention in early diagnosis and therapy of cancer. In this work, we develop a novel aptamer-guided nanocarrier based on the mesoporous metal-organic framework (MOF) shell and up-conversion luminescent $NaYF_4$:Yb^{3+}/Er^{3+} nanoparticles (UCNPs) core for the first time to achieve these goals. These UCNPs, chosen as optical labels in biological assays and medical imaging, could emit strong green emission under 980 nm laser. The MOF structure based on iron (III) carboxylate materials [MIL-100 (Fe)] possesses high porosity and non-toxicity, which is of great value as nanocarriers for drug storage/delivery. As a unique nanoplatform, the hybrid inorganic-organic drug delivery vehicles show great promising for simultaneous targeted labeling and therapy of cancer cells.

Recently, the development of novel nanoparticles (NPs) with unique biological properties has spurred tremendous research interest in the field of nanomedicine[1]. As a medical nanoplatform, the design of multifunctional NPs which could not only carry small drug molecules for therapeutics but also be imaging agents for detecting cancer at the molecular level, is still an open challenge. In this field, nano-sized metal-organic frameworks (MOFs) based on iron (III) carboxylate materials with different compositions and structures (e.g. MIL-100, MIL-101; MIL = Materials of Institute Lavoisier), have potential applications in biomedicine due to their acceptable *in vitro* and *in vivo* toxicological results[2–4]. Serving as nanocarriers for guest molecules, iron (III) carboxylate MOFs display several fascinating features including high pore volume and tunable pore size for efficient payloads and unconspicuous burst effect of entrapped drugs[5,6], a large variety of structural topologies and compositions for decorating the frameworks with functional groups or molecules[7]. In order to design of multi-functional MOF-base nanocarriers for bioapplication, incorporating NPs with unique optical properties within MOFs is indeed an effective strategy.

Lanthanide-doped upconversion nanoparticles (UCNPs) are confirmed an excellent functional agent as the core scaffolds of core-shell materials with outstanding optical imaging property[8,9]. Such UCNPs, capable of converting near-infrared radiation to visible lights, have become a new generation of bioprobes in biomedical applications[10–13]. Their unique optical properties provide minimal autofluorescence background, deep light penetration depth and minimal photo-damage to living organisms for *in vivo* optical imaging and bioassay[14,15]. Moreover, drug nanocarriers could be uptaken into a cell by the endocysis pathway. To endow them with specific recognition ability are indeed vital and meaningful to reduce unwanted side-effects on normal cells during cancer therapy[16]. Small molecules as targeting ligands (folic acid[17], RGD peptide[18], aptamers[19]) were incorporated into these drug delivery system. Aptamers, with highly specific binding to a target of interest (small molecules, proteins, and even cancer cells)[20,21], have become one of the most promising techniques for introducing target moiety to nanomaterials.

Here, we first report the core-shell UCNPs@MOF nanocomposites (NCs) with β-$NaYF_4$:Yb^{3+}/Er^{3+} core (the most efficient UCNPs) and MIL-100 (Fe) shell prepared via facile two-step approach. This simple and green method is based on the interaction between UCNPs and MOF precursor at room temperature. By covalently conjugated on the surface of UCNPs@MOF NCs, AS1411 aptamer could make it possible for targeting cancer cell. The procedure for synthesis of UCNPs@MOF-DOX-AS1411 nanocarriers is summarized as shown in Figure 1. MOF shell could be specifically formed on the surface of UCNPs by self-assembly of Fe^{3+} ions and carboxylic

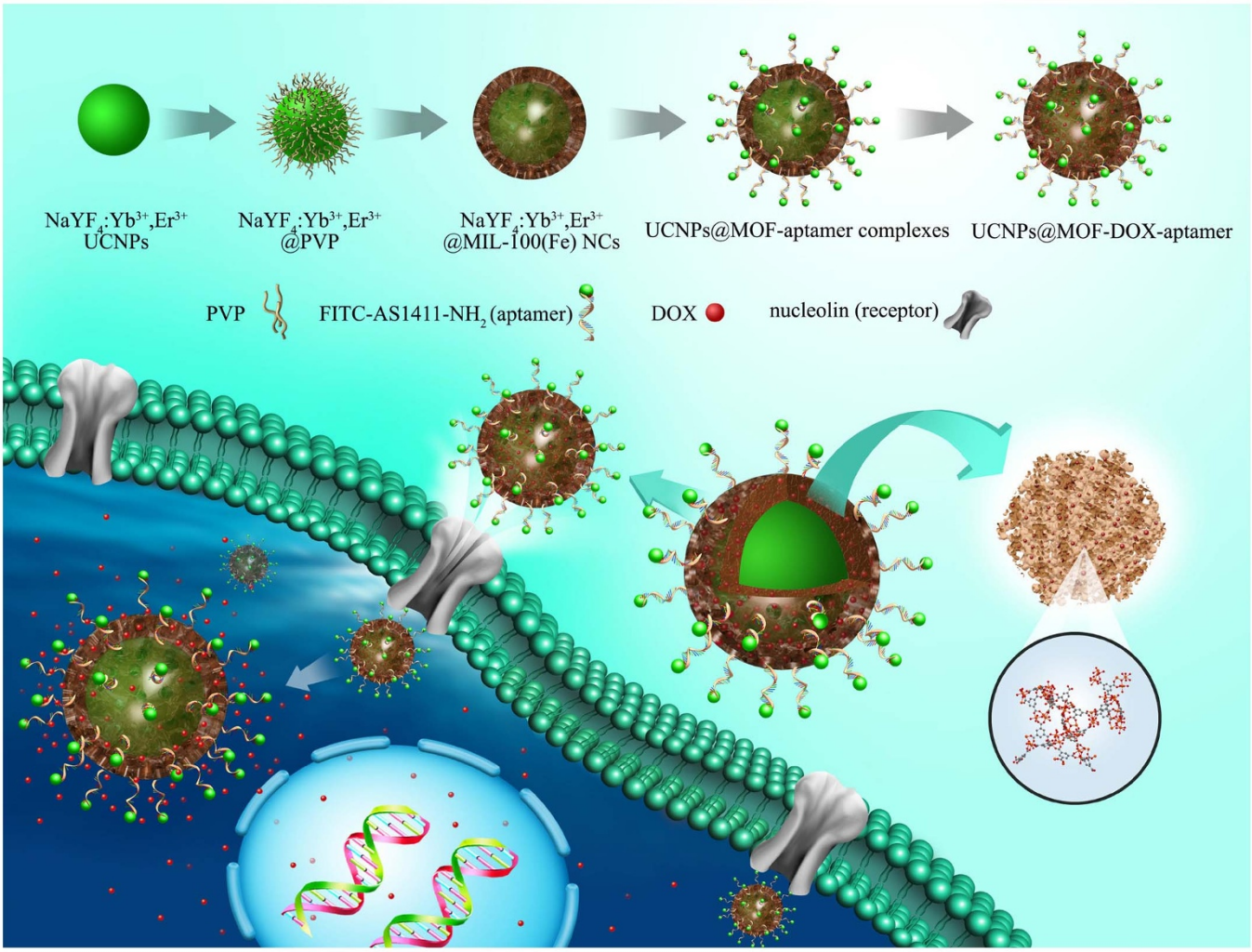

Figure 1 | Schematic illustration of the synthetic procedure. Synthetic procedure, anti-tumor drug loading and possible receptor-mediated endocytosis pathway of the targeted UCNPs@MOF core–shell NCs. The insets were expanded view of the porous cavities of MIL-100(Fe) and part coordination structure, respectively.

acid[22]. Anticancer aptamer AS1411 (a 26-mer guanine-rich oligonucleotide), was chosen for targeting cancer cells and enhancing intracellular uptake, since it can bind to nucleolin (a receptor for AS1411 and overexpressed on the plasma membrane of tumor cells[23]) with high affinity and specificity. At the 5′ end of AS1411 aptamer, fluorescein isothiocyanate (FITC) was decorated for fluorescence labeling, meanwhile at the 3′ terminal amino groups (-NH_2) were linked for being the anchor of this aptamer. Subsequently, anticancer drug DOX-loaded UCNPs@MOF NCs could specifically recognize cancer cells and go across the cell membrane by possible receptor-mediated endocytosis pathway. In agreement with such views, the hybrid nanoplatform exhibits up-conversion fluorescence imaging under 980 nm laser for *in vitro* cell imaging and drug could be carried to selective cancer cells. It shows a promising strategy for increasing chemotherapeutic efficiency and monitoring cancer progression simultaneously.

Results

Preparation and Characterizations of UCNPs@MOF NCs. The physicochemical characteristics of as-obtained core-shell UCNPs@MOF NCs were examined by transmission electron microscope (TEM), X-ray diffraction (XRD), Fourier transform Infrared spectra (FT-IR) and X-ray photoelectron spectroscopy (XPS). TEM images (Figure 2) show the uniform morphology and good monodispersity of PVP-modified UCNPs with a size around 30 nm. After mixing with MOF precursor solution for different reaction times, the particle sizes of UCNPs@MOF NCs increase gradually (Figure 2b–c). It presents a thicker nanolayer (~8 nm) coating on the UCNPs@MOF NCs after 1.5 h growth of reaction time, indicating the formation of MOF shell functioning as drug containers. The dynamic light scattering data (Figure S1) have shown the hydrodynamic size and size distribution of the samples in different physiological solutions. The results indicated that the average size of UCNPs@MOF NCs in deionized water (A) is 138.8 nm while in cell culture media containing FBS (B) is 125.1 nm. Furthermore, the core-shell structure of the UCNPs@MOF NCs can be further confirmed by the low-magnification high angle annular dark field scanning TEM (HAADF–STEM) image (Figure 2d), which clearly shows the contrast between the shell (bright) and core (dark). The EDS line scanning profiles present the elements Y and Fe, which are peculiarly dispersed in the core and shell, respectively. The XRD pattern (Figure S2) proves the formation of the UCNPs@MOF nanocomposites. The peaks of both β-$NaYF_4$ (JCPDS No. 16-0334) and MIL-100(Fe) appeared.

The surface property of as-synthesized UCNPs@MOF NCs was monitored by FT-IR spectrum (Figure S3). The broad band at 3404 cm^{-1} corresponds to ν(O-H), and the weak band at 1723 cm^{-1} is assigned to ν(C=O), implying the loss of most of free carboxyl groups compared with the raw material H_3BTC. The residual carboxyl groups make it possible for introducing functional

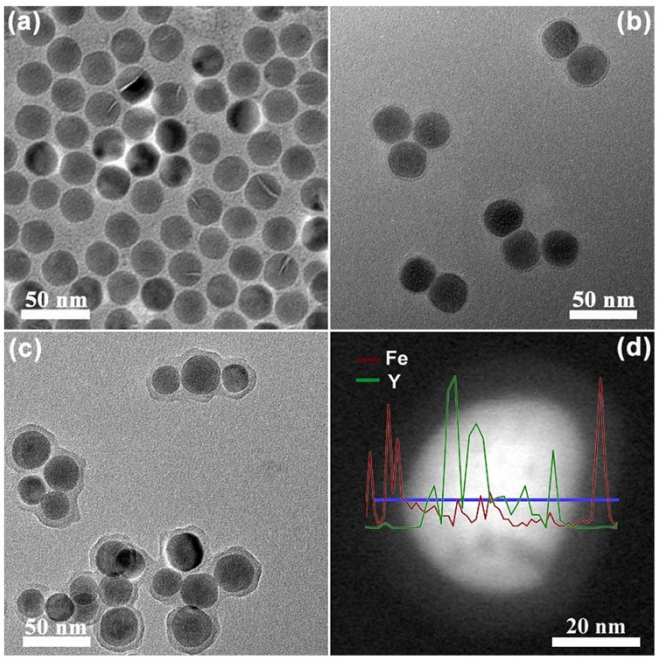

Figure 2 | Structural characterization. TEM images of β-$NaYF_4$:Yb^{3+}/Er^{3+} NPs (a) and the core–shell structured UCNPs@MOF NCs with different reaction time (b for 40 min, c for 90 min). HAADF-STEM images of UCNPs@MOF NCs (d). The inset in d is corresponding EDS line scanning profiles.

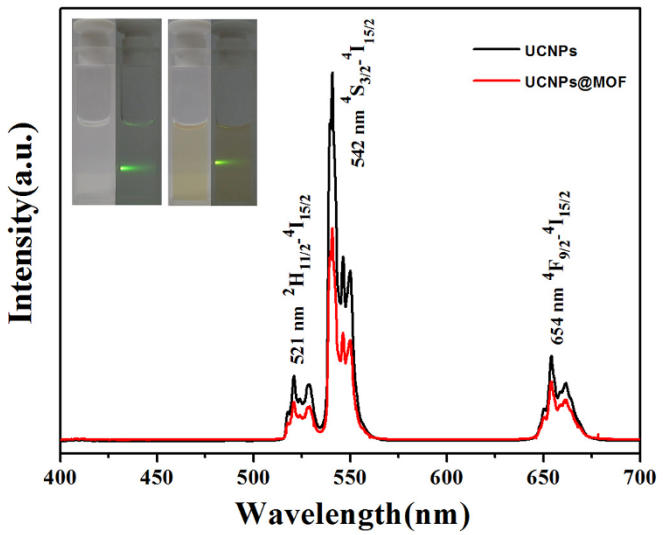

Figure 3 | Optical properties. The UC emission spectra of pure UCNPs and the UCNPs@MOF NCs dispersed in ethanol solution under excitation of 980 nm. The inset is corresponding luminescent photographs of pure UCNPs (right) and the UCNPs@MOF NCs (left) in ethanol solution with 980 nm laser irradiation, respectively.

group into the as-prepared samples. These results confirm the coordination compound of carboxyl group and Fe ions. To determine qualitatively the surface component and the composition, the survey XPS spectra of as-prepared UCNPs@MOF sample (Figure S4) was performed. Note that among these peaks, two peaks at the binding energies of 725 and 712 eV can be assigned to Fe $2p_{1/2}$ and Fe $2p_{3/2}$, respectively[24]. The weak signals of the elements belonging to the cores (Na, Y, F) maybe result from the detection depth of XPS. The porosity feature of the MIL-100(Fe) shells determine the drug loading property of the core–shell UCNPs@MOF NCs. Porosity of as-obtained UCNPs@MOF NCs (Figure S5) was revealed by N_2 sorption isotherms. It shows typical type IV isotherms with H1 hysteresis loop, which indicates the mesopores of UCNPs@MOF NCs. The pore volumes and the BET surface areas of core–shell NCs were determined to be 0.42 $cm^3 \cdot g^{-1}$ and 586 $m^2 \cdot g^{-1}$, respectively. Furthermore, the pore size distribution of the UCNPs@MOF NCs estimated by BJH method exhibit an apex centered at 2.8 nm, which makes them as an efficient nanocarrier for drug loading and delivery. Figure 3 presents the up-converting emission spectra and corresponding luminescent photographs of the PVP-capped *β*-$NaYF_4$:Yb^{3+}/Er^{3+} UCNPs and UCNPs@MOF NCs. Both of the samples can be well-dispersed in the ethanol and exhibit green emission under the excitation of 980 nm NIR laser (insets of Figure 3). The emission spectrum contains three primary peaks: a strong peak at 542 nm, a moderate peak at 654 nm and a weak peak at 521 nm, consisting with the transitions of Er^{3+} ions from $^2H_{11/2}$ to $^4I_{15/2}$, from $^4S_{3/2}$ to $^4I_{15/2}$, from $^4F_{9/2}$ to $^4I_{15/2}$, respectively[25]. The slight decrease of luminescence intensity of UCNPs@MOF NCs is in accordance with the result that the MIL-100(Fe) shells were coated on the surface of PVP-capped *β*-$NaYF_4$:Yb^{3+}/Er^{3+} UCNPs.

***In vitro* Cytotoxicity and Drug Loading/Release of UCNPs@MOF NCs.** Previous reports have evidenced that the lanthanides based UCNPs and iron (III) carboxylate MOFs exhibit no or low cytotoxicity *in vivo*[26,27]. The obtained UCNPs@MOF NCs were incubated with 293 cells, and the standard MTT assay was used for the study on the cell viability of UCNPs@MOF NCs. Cell viability is directly proportional to the amount of formazan produced monitored by the absorbance at 490 nm. The UCNPs@MOF NCs were delivered over a range of dosages (25–1000 $\mu g \cdot mL^{-1}$). More than 94% cells viabilities were observed under the varying concentration range (Figure S6), indicating that UCNPs@MOF NCs have no significant cytotoxic effect in all dosages. A model drug DOX was loaded into the pores of UCNPs@MOF NCs, and the loading ratio was calculated to be 17.2 wt% by measuring the characteristic DOX optical absorbance at 480 nm. The high payload of DOX is attributed to exceptional porosity of MIL-100(Fe) shells. Figure S7 depicts the DOX release profiles of DOX-loaded UCNPs@MOF in PBS buffer of different pH values (7.4 and 5.0) at 37°C. It has been noteworthy that unconspicuous burst effect and inconceivably slow DOX release that lasts as long as for 35 days for UCNPs@MOF-DOX NCs in PBS solution, demonstrating the loaded DOX mostly distribute within the channels and cavities of MOF shells. The faster release rate in low pH values is observed, since about 18% of DOX released in neutral PBS (pH = 7.4) in 4 days while the same amount just in the first 2 h in acidic PBS (pH = 5.0). Due to degradation of MOF shell in some extent in PBS solution[28], the released DOX increases with continuously degradation of MOF structure. After incubating with UCNPs@MOF-DOX NCs in PBS (pH = 7.4) for 6 h, 12 h, 24 h, 36 h, 72 h and 108 h, the Fe concentrations in supernatants determined by ICP-MS were to be 2.9, 4.6, 5.6, 6.5, 7.8 and 9.7 $\mu g \cdot mL^{-1}$, respectively. It could be confirmed that the degradation degree of MOF shell in PBS gradually increases with prolonging incubation times. The surface zeta-potential of the UCNPs@MOF NCs in these PBS solutions were measured, which showed the surface charge of NCs was −6.5 mV in PBS of pH = 5.0 and −11.7 mV in PBS of pH = 7.4, respectively. Thus, the pH-sensitive DOX release could be speculated for that the surface zeta-potential of the UCNPs@MOF samples become more positive in the acidic condition, and the weaker electrostatic adherence between MOF and positive-charged DOX might lead to the faster drug release[29].

Targeted cellular uptake and biological imaging of aptamer-mediated UCNPs@MOF NCs. Aptamers-functionalized up-conversion luminescent nanomaterials as signal reporting groups

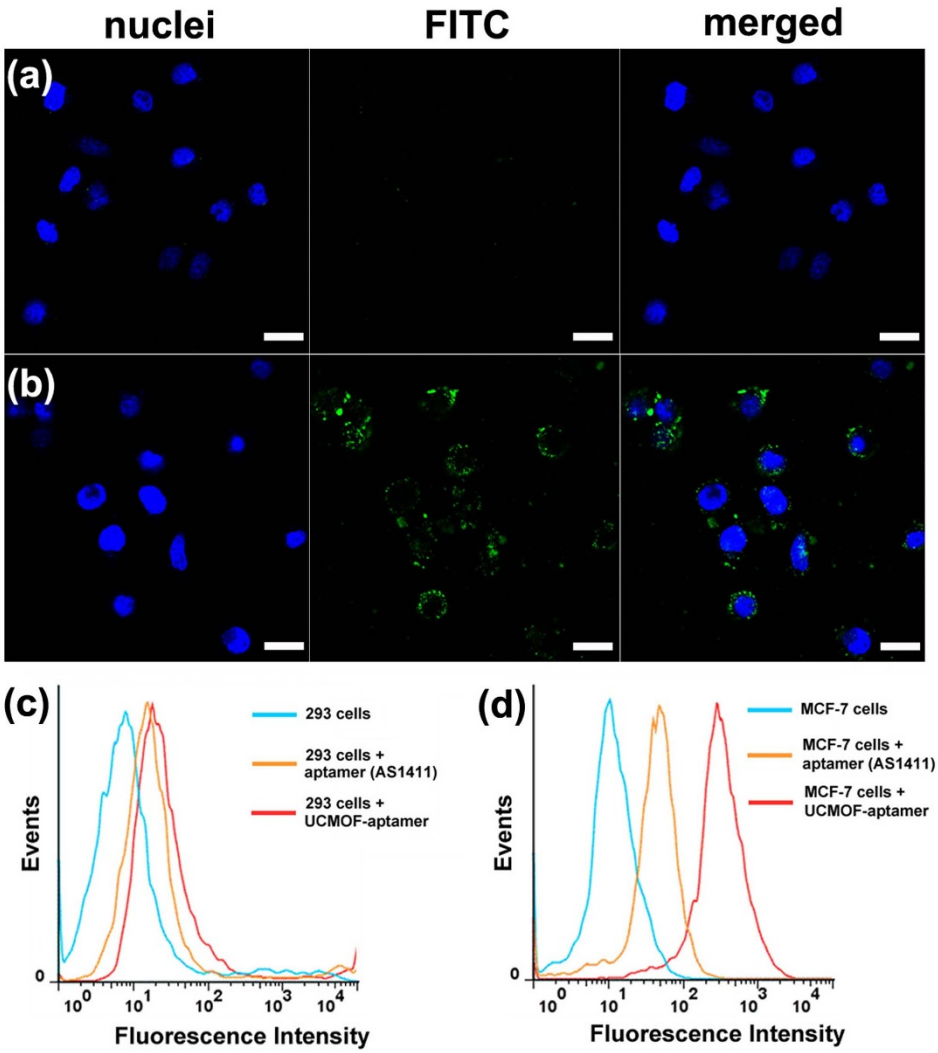

Figure 4 | CLSM and flow cytometry analysis. The confocal laser scanning microscopy (CLSM) images of 293 cells (a) and MCF-7 cells (b) incubated with UCNPs@MOF-DOX-AS1411 NCs for 1 h at 37°C. Each series can be sorted by the nuclei of cells being dyed in blue by Hoechst 33324, FITC labeled UCNPs@MOF-DOX-AS1411 NCs and a merge of the two channels of both above, respectively. All scale bars are 20 μm. Flow cytometry analysis to monitor the binding of aptamer (AS1411-FITC) and UCNPs@MOF-DOX-AS1411 NCs with 293 cells (c; control cells) and MCF-7 cells (d; target cells) for 20 min, respectively.

therefore develops a novel and potential diagnostic tool for the detection of cancer in early stage[20]. In our design, the UCNPs@MOF NCs with carboxyl groups on the surface were conjugated to 3′-amine-functionalized AS1411 aptamers by carbodiimide coupling chemistry. Meanwhile, the fluorescein isothiocyanate (FITC) was labeled at the 5′ end of AS1411 aptamers as fluorescent probe. MCF-7 cells (human breast cancer cells) with nucleolin over expression was served as the target cancer cell and 293 cells (Human Embryonic Kidney cells) without nucleolin expression was selected as a negative control cell. The confocal laser scanning microscopy (CLSM) images of 293 cells (a) and MCF-7 cells (b) cultured with FITC labeled UCNPs@MOF-AS1411 NCs for 1 h are shown in Figure 4. As we see, the strong fluorescence signals were observed from the MCF-7 cancer cell zone, but no noticeable fluorescence from the 293 cell zone. It was inferred that the UCNPs@MOF-AS1411 NCs were mostly internalized into the cells by the efficient way of receptor-mediated endocytosis. The targeting specificities of UCNPs@MOF-AS1411 NCs toward MCF-7 cells were further confirmed by flow cytometry, AS1411 aptamer was used as a positive control. After incubating the FITC labeled AS1411 aptamers and UCNPs@MOF-AS1411 NCs both with 293 cells and MCF-7 cells for 30 min, little binding shift happened in the controlled cells (293 cells, Figure 4c), while obvious binding shift was observed in the targeting cells (MCF-7 cells, Figure 4d). It was noticeable that UCNPs@MOF-AS1411 NCs exhibited stronger binding with MCF-7 cells than free aptamers. It may be attributed to the multivalent effect that the affinity of a ligand to its receptor is highly dependent on the three-dimensional arrangement and its valency (the number of sites available for receptor attachment)[30,31]. Therefore, multiple targeting ligands on the surface of UCNPs@MOF-aptamer lead to the greater binding avidity, and enhance specific binding affinity. These results demonstrated that the aptamers mediated UCNPs@MOF NCs could be effectively taken up and internalized by target cancer cells with high selectivity but presented little affinity to non-target normal cells.

Furthermore, the interactions of *in vitro* cells with UCNPs@MOF-AS1411 NCs were investigated by up-conversion luminescent microscopy (UCLM). The up-conversion luminescence images of 293 cells and MCF-7 cells incubated with UCNPs@MOF-AS1411 NCs (Figure 5) were taken by a modified inverted fluorescence microscopy equipped with infrared laser excitation at 980 nm. The green UC luminescence signals of UCNPs@MOF-AS1411 NCs can be observed. Overlaying the nuclei of cells with UC luminescent images further demonstrates that the observed green luminescence is

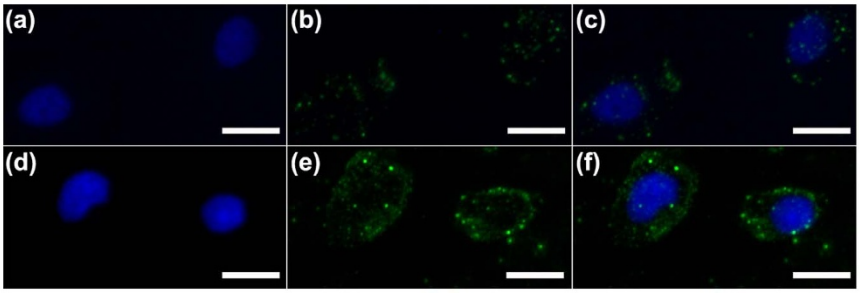

Figure 5 | UC Luminescent Imaging. Inverted florescence microscope images of 293 cells (a–c) and MCF-7 cells (d–f) incubated with UCNPs@MOF-DOX-AS1411. Each series can be classified to the nuclei of cells being dyed in blue by Hoechst 33324 (a, d), up-conversion luminescent images (b, e) and overlay of above (c, f). All scale bars are 20 μm.

localized in the cytoplasm of cells. It should be noted that the stronger luminescence signals were detected in the MCF-7 cells due to the receptor-mediated endocytosis, agreeing well with the CLSM and flow cytometry results. More importantly, the results of UCLM confirm that $NaYF_4$:Yb^{3+}/Er^{3+} UCNPs, which are the cores of UCNPs@MOF-AS1411 NCs, can be directly used as biological fluoresce probes without modifying other fluorescent organic molecules on the AS1411 aptamers.

***In vitro* cytotoxicity effect on target/normal cells of aptamer-mediated DOX-UCNPs@MOF NCs.** *In vitro* cell viabilities of pure UCNPs@MOF, UCNPs@MOF-DOX and UCNPs@MOF-DOX-AS1411 with various concentrations on 293 cells (a) and MCF-7 cells (b) were evaluated by MTT assay (Figure 6). Both cell lines treated with pure UCNPs@MOF show negligible cell death even at concentrations up to 1000 $\mu g \cdot mL^{-1}$, thus indicating good biocompatibility of the nanocomposites. In contrast, the UCNPs@MOF-DOX and UCNPs@MOF-DOX-AS1411 show increasing inhibition effect against both 293 cells and MCF-7 cells with the increase of loaded DOX concentration. About 32% of 293 cells and 44% MCF-7 cells were killed under 1000 $\mu g \cdot mL^{-1}$ of UCNPs@MOF-DOX at an equivalent DOX concentration of 170 $\mu g \cdot mL^{-1}$, respectively. Due to the low-pH induced faster release of the loaded DOX inside the endosomal compartment of the cancer cells, the higher cytotoxicity of UCNPs@MOF-DOX on MCF-7 cells than that on 293 cells was observed. Compared with UCNPs@MOF-DOX, aptamer-mediated UCNPs@MOF-DOX-AS1411 showed higher cytotoxicity with MCF-7 cells, whereas the cytotoxicity of UCNPs@MOF-DOX-AS1411 incubated with 293 cells had no obvious variation. The greater cytotoxic effect of UCNPs@MOF-DOX-AS1411 on MCF-7 cells can be explained that AS1411 aptamer functionalization enables specific binding to the target MCF-7 cells following by selective internalization of the nanocomposites.

Discussion

In this work, the UCNPs@MOF multifunctional nanocomposites with the up-conversion luminescent $NaYF_4$:Yb^{3+}/Er^{3+} nanoparticles (UCNPs) core and mesoporous MIL-100(Fe) shell were first prepared by facile green synthesis. The hydrophobic UCNPs were removed the oleic acid ligands by the ultrasonic treatment in the acid solution. In order to provide the enhanced affinity between UCNPs and MIL-100(Fe), polyvinylprolidine (PVP) was capped onto the surface of UCNPs core for the coordination interactions of pyrrolidong rings and Fe^{3+} ions[24,32]. It can also be found that PVP acts as stabilizing reagent in the reaction solution to improve the dispersion of UCNPs (compared with Figure S8). As-obtained core-shell UCNPs@MOF nanocomposites exhibit unique up-converting green emission under laser excitation at 980 nm. Compared with the photobleaching and quenching of fluorescent organic molecules, the toxicity of semiconductor quantum dots, and high auto-fluorescence background of down-conversion luminescence materials, the UCNPs@MOF up-conversion luminescent nanocomposites provide the possible optical imaging for *in vivo* bioprobes.

The cytotoxicity of the nanocomposites would be crucial factor in evaluating the potential biomedical applications. Nontoxic UCNPs@MOF NCs are suitable for serving as drug carriers. We estimated the

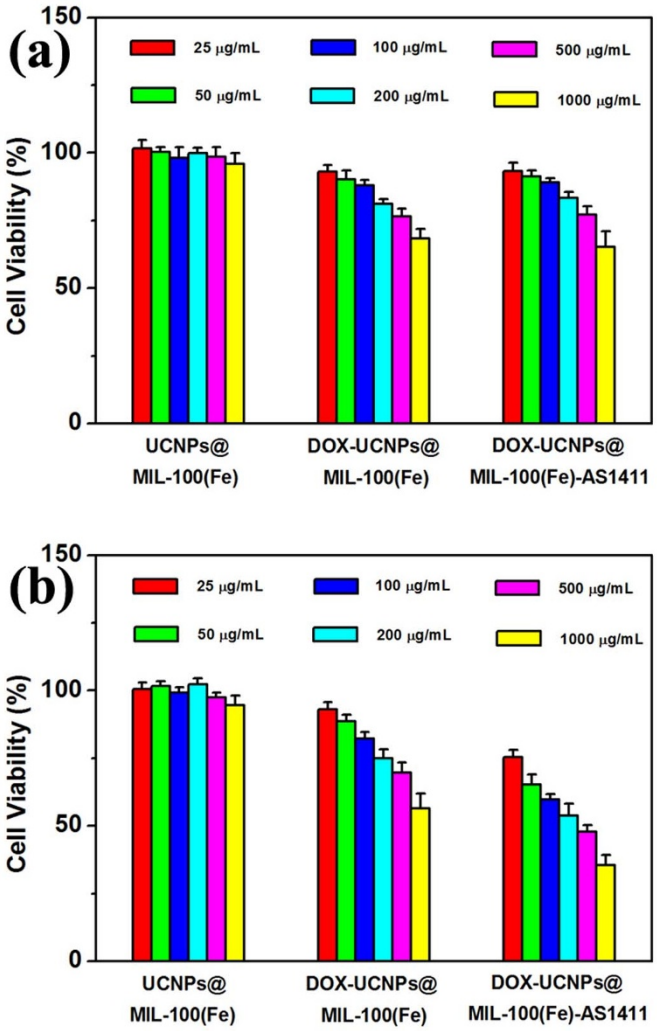

Figure 6 | The targeted pharmacological efficacy. *In vitro* cell viabilities after incubation for 24 h with pure UCNPs@MOF NCs, UCNPs@MOF-DOX and UCNPs@MOF-DOX-AS1411 at different concentrations to Human Embryonic Kidney 293 cells (a) and MCF-7 cancer cells (b) measured by MTT assay, respectively.

drug (DOX) loading and release behaviors of UCNPs@MOF NCs in phosphoric buffer solutions (PBS) with two different pH values. It shows the pH-sensitive drug release, which might be beneficial to induce cell death at the reduced pH values in intracellular endosomes/lysosomes and certain weakly acidic environment of cancerous tissues. AS1411, binding to the receptor nucleolin on the cancer cell surface with high affinity and selectivity, was used to modify the UCNPs@MOF NCs with the capability of targeted biological imaging. By grafting AS1411 aptamers upon UCNPs@MOF NCs, target-specific drug delivery was achieved. The targeted pharmacological efficacy of aptamer-mediated and DOX loaded UCNPs@MOF NCs was investigated by MTT assay. The enhenced and selective cytotoxicity to target cancer cells, as well as reduced the side effects in normal cells validates the possibility of aptamers-mediated UCNPs@MOF-DOX drug delivery system for bioapplication.

Therefore, it confirms that the hybrid nanocarriers for chemotherapeutic drugs possess not only high cell biocompatibility and pH-sensitive entrapped drug release, but also *in vitro* targeted up-converting imaging and drug delivery to selective cancer cells. We envision that this aptamer-mediated UCNPs@MOF nanoplatform shows promise in the way of associate targeted cancer therapeutics and diagnostics.

Methods

Synthesis of oleic acid stabilized β-$NaYF_4$:Yb^{3+}/Er^{3+} nanoparticles. Oleic acid stabilized β-$NaYF_4$:Yb^{3+}/Er^{3+} NPs were prepared by thermal decomposition methodology according to previous reports in literature[33]. Typically, 1 mmol $RE(oleate)_3$ (RE = 78%Y + 20% Yb + 2%Er), 12 mmol of NaF solid powder, 10 mL of OA and 10 mL of ODE were added into the a 100 mL three-necked flask. The mixture were heated to 110°C and degassed under vacuum with vigorous magnetic stirring for about 30 min and then flushed with N_2. Then the temperature of the reaction was kept at 320°C for 1.5 h in N_2 atmosphere under vigorous stirring. As the reaction mixture was cooled to 60°C, the NPs were precipitated by the addition of ethanol and separated by centrifugation. The finally obtained NPs were dispersed in cyclohexane for further use.

Preparation of water-soluble and PVP-capped β-$NaYF_4$:Yb^{3+}/Er^{3+} nanoparticles. The as-prepared β-$NaYF_4$:Yb^{3+}/Er^{3+} NPs were dispersed in 5 mL (0.1 M) dilute hydrochloric acid solution and sonicated for 5 h and then washed three times with distilled water. Subsequently, the products were dissolved in 8 mL of ethanol containing 1.6 g PVP. After vigorous stirring, PVP- capped β-$NaYF_4$:Yb^{3+}/Er^{3+} NPs were obtained.

Synthesis of β-$NaYF_4$:Yb^{3+}/Er^{3+}@MIL-100(Fe) nanocrystals. 2 mL above absolute ethanol was firstly added dropwise into a round-bottom flask containing 4 mL of $FeCl_3 \cdot 6H_2O$ DMF solution (10 mM) for 15 minutes and then 4 mL trimesic acid ethanol solution (10 mM) added for 40 min (or 1.5 h) at 25°C under stirring. To remove redundant iron ions and acid, these NPs were washed two times with ethanol by centrifuged.

Preparation of UCNPs@MOF-DOX-AS1411 nanocomposites. β-$NaYF_4$:Yb^{3+}/Er^{3+}@MIL-100(Fe) NCs were first dispersed in 5 mL of ethanol solution with 5 mg EDC and 2.5 mg NHS under strong agitation for 24 h. After separated by centrifugation and washed with deionized water, the precipitations were added in the PBS solution (2 mL; 5 mM, pH7.4; containing 2.5 mM $MgCl_2$, 140 mM KCl) in which AS1411 aptamer were first added and stirred for 2 h. After standing in 4°C overnight, the β-$NaYF_4$:Yb^{3+}/Er^{3+}@MIL-100(Fe)-AS1411 samples were isolated by centrifugation and washed by PBS buffer. By adding the samples into 2 mL DOX aqueous solution (1 $mg \cdot mL^{-1}$), the UCNPs@MOF-DOX-AS1411 complexes were obtained.

Drug storage/delivery studies. 10 mg UCNPs@MOF NCs dispersed in 4 mL DOX aqueous solution (1 $mg \cdot mL^{-1}$). The DOX-loaded sample was collected by centrifugation after constant stirring for 24 h under dark conditions. The drug release was studied by suspending the DOX-loaded sample in 3 mL of a phosphate buffer solution (PBS, pH 7.4 and 5.0) at 37°C with gentle shaking. At each time point time, PBS was taken and replaced with an equal volume of fresh PBS. Released DOX was quantified in the supernatant by UV-vis spectrophotometer.

***In vitro* cytotoxicity assays of UCNPs@MOF NCs.** *In vitro* cytotoxicity of UCNPs@MOF NCs was evaluated by MTT assays against the Human Embryonic Kidney 293 cells and human breast cancer MCF-7 cells. Briefly, 293 cells and MCF-7 cells were seeded in a 96-well plate in which cells density is 5000 cells per test well, and cultured overnight at 37°C in a 5% CO_2 incubator. The DOX-loaded UCNPs@MOF NCs and UCNPs@MOF-AS1411 were added to respective test well and the cells were cultured for 24 h in 5% CO_2. The concentrations of the nanocrystals were 25, 50, 100, 200, 500, 1000 $\mu g \cdot mL^{-1}$, respectively. Following incubation, the medium containing the UCNPs@MOF NCs was removed, and MTT solution (20 μL) was added into each cell and cultured for another 4 h. Then the supernatant was replaced with 150 μL of dimethyl sulfoxide (DMSO) each well, following by monitored using a microplate reader (Therom Multiskan MK3) at 490 nm. The cytotoxicity was estimated by the percentage of cell viability compared to untreated control cells.

Cellular uptake of UCNPs@MOF NCs. Cellular uptake was examined using confocal laser scanning microscope (CLSM) and flow cytometry. For CLSM, 293 cells and MCF-7 cells were seeded in 6-well culture plates and were cultured overnight. After incubated with UCNPs@MOF-AS1411 NCs at 37°C for 2 h in the dark, for removing the residual nanocrystals, the cells were washed with PBS several times, and then fixed with 2.5% formaldehyde at 37°C for 10 min before washing with PBS again. Hoechst 33342 solution was used for nucleus labeling of fixed cells for 10 min, and then the cells were washed with PBS several times. Lastly, the cells were visualized under CLSM after the cover slips were placed on a glass microscope slide. For flow cytometry analysis, the 293 and MCF-7 cells were seeded in 6-well culture plates (1×10^6 per well) and grown overnight. The cells were incubated with UCNPs@MOF-AS1411 NCs at 37°C for 30 min. After prepared consecutively by trypsinization, and washed with PBS, a single cell suspension was filtrated through 35 mm nylon mesh. Then, the cells were lifted by using a cell stripper (Media Tech. Inc.), and then analyzed using a flow cytometer (FACSCalibur, BD Biosciences) for FITC.

UC Luminescent Imaging of the UCNPs@MOF-DOX-AS1411 NCs. The up-conversion luminescence microscopy (UCLM) instrument equipped with an inverted fluorescence microscope (Nikon Ti-S) and an external CW 980 nm laser diode was available for illuminating upon the samples. 5×10^4 per well of MCF-7 cells were seeded in 6-well culture plates and were cultured overnight. After incubated with UCNPs@MOF-AS1411 NCs at 37°C for 4 h, all the cells washed with PBS solution. The cells were fixed with 2.5% formaldehyde at 37°C for 10 min, and then washed with PBS solution. UCLM imaging was performed with the reconstructive microscope and cells were treated by infrared laser (BWT Beijing LTD, China) at 980 nm with output power of 250 mW.

Characterization of the samples. The X-ray diffraction date were collected in a D8 Advanced diffractometer (Bruker) using CuKα radiation (λ = 0.154 nm). Transmission electron microscopy measurements were carried out on a FEI Tecnai G2 S-Twin with a field emission gun operating at 200 kV. Dynamic light scattering (DLS) and surface zeta potential measurements were performed on a Malvern instrument Zatasizer Nano. N_2 adsorption/desorption analysis was measured on a Micromeritics ASAP 2020M apparatus. The Brunauer-Emmett-Teller (BET) method was used to calculate the specific surface area of samples from the data between 0.05 and 0.35, and t-plot method was to calculate the pore volume. The UV-vis absorption spectra were obtained from U-3100 spectrophotometer (Hitachi). Fourier transform Infrared spectra (FT-IR) were obtained by a PerkinElmer 580BIR spectrophotometer using KBr pellets. The X-ray photoelectron spectra (XPS) were performed on an ECSALAB 250. The UC emission spectra were carried out from an F-7000 fluorescence spectrometer (Hitachi) using a 980 nm laser as the excitation source. The digital photos of up-converting luminescence were obtained from a Canon camera. CLSM images were acquired from a FV 1000 confocal laser scanning microscrope (Olympus). A flow cytometry was recorded on a FCM cytometer (BD Biosciences) using 488 nm as excitation wavelength.

1. Thakor, A. S. & Gambhir, S. S. Nanooncology: The future of cancer diagnosis and therapy. *CA Cancer J. Clin.* **63**, 395–418 (2013).
2. McKinlay, A. C. *et al.* BioMOFs: Metal–organic frameworks for biological and medical applications. *Angew. Chem. Int. Ed.* **49**, 6260–6266 (2010).
3. Della Rocca, J., Liu, D. & Lin, W. Nanoscale metal–organic frameworks for biomedical imaging and drug delivery. *Acc. Chem. Res.* **44**, 957–968 (2011).
4. Tamames-Tabar, C. *et al.* Cytotoxicity of nanoscaled metal-organic frameworks. *J. Mater. Chem. B* **2**, 262–271 (2014).
5. Chalati, T. *et al.* Porous metal organic framework nanoparticles to address the challenges related to busulfan encapsulation. *Nanomedicine* **6**, 1683–1695 (2011).
6. Horcajada, P. *et al.* Metal–organic frameworks as efficient materials for drug delivery. *Angew. Chem. Int. Ed.* **45**, 5974–5978 (2006).
7. Horcajada, P. *et al.* Extended and functionalized porous iron(iii) tri- or dicarboxylates with MIL-100/101 topologies. *Chem. Commun.* **50**, 6872–6874 (2014).
8. Liu, J., Bu, W., Pan, L. & Shi, J. NIR-triggered anticancer drug delivery by upconverting nanoparticles with integrated azobenzene-modified mesoporous silica. *Angew. Chem. Int. Ed.* **52**, 4375–4379 (2013).
9. Feng, W., Han, C. & Li, F. Upconversion-nanophosphor-based functional nanocomposites. *Adv. Mater.* **25**, 5287–5303 (2013).
10. Dai, Y. *et al.* In vivo multimodality imaging and cancer therapy by near-infrared light-triggered trans-platinum pro-drug-conjugated upconverison nanoparticles. *J. Am. Chem. Soc.* **135**, 18920–18929 (2013).
11. Sun, Y., Zhu, X., Peng, J. & Li, F. Core–shell lanthanide upconversion nanophosphors as four-modal probes for tumor angiogenesis imaging. *ACS Nano* **7**, 11290–11300 (2013).

12. Wang, C., Cheng, L. & Liu, Z. Drug delivery with upconversion nanoparticles for multi-functional targeted cancer cell imaging and therapy. *Biomaterials* **32**, 1110–1120 (2011).
13. Cheng, L. *et al.* Multifunctional nanoparticles for upconversion luminescence/MR multimodal imaging and magnetically targeted photothermal therapy. *Biomaterials* **33**, 2215–2222 (2012).
14. Wang, F. & Liu, X. Recent advances in the chemistry of lanthanide-doped upconversion nanocrystals. *Chem. Soc. Rev.* **38**, 976–989 (2009).
15. Sun, L.-D., Wang, Y.-F. & Yan, C.-H. Paradigms and challenges for bioapplication of rare earth upconversion luminescent nanoparticles: small size and tunable emission/excitation spectra. *Acc. Chem. Res.* **47**, 1001–1009 (2014).
16. Shangguan, D. *et al.* Aptamers evolved from live cells as effective molecular probes for cancer study. *Proc. Natl. Acad. Sci.* **103**, 11838–11843 (2006).
17. Cheng, L. *et al.* Facile preparation of multifunctional upconversion nanoprobes for multimodal imaging and dual-targeted photothermal therapy. *Angew. Chem. Int. Ed.* **50**, 7385–7390 (2011).
18. Rieter, W. J., Pott, K. M., Taylor, K. M. L. & Lin, W. Nanoscale coordination polymers for platinum-based anticancer drug delivery. *J. Am. Chem. Soc.* **130**, 11584–11585 (2008).
19. Tong, G. J., Hsiao, S. C., Carrico, Z. M. & Francis, M. B. Viral capsid DNA aptamer conjugates as multivalent cell-targeting vehicles. *J. Am. Chem. Soc.* **131**, 11174–11178 (2009).
20. Xing, H., Wong, N. Y., Xiang, Y. & Lu, Y. DNA aptamer functionalized nanomaterials for intracellular analysis, cancer cell imaging and drug delivery. *Curr. Opin. Chem. Biol.* **16**, 429–435 (2012).
21. Liang, H. *et al.* Functional DNA-containing nanomaterials: cellular applications in biosensing, imaging, and targeted therapy. *Acc. Chem. Res.* **47**, 1891–1901 (2014).
22. Cunha, D. *et al.* Rationale of drug encapsulation and release from biocompatible porous metal–organic frameworks. *Chem. Mater.* **25**, 2767–2776 (2013).
23. Soundararajan, S., Chen, W., Spicer, E. K., Courtenay-Luck, N. & Fernandes, D. J. The nucleolin targeting aptamer AS1411 destabilizes Bcl-2 messenger RNA in human breast cancer cells. *Cancer Res.* **68**, 2358–2365 (2008).
24. Zhang, Z. *et al.* Well-defined metal–organic framework hollow nanocages. *Angew. Chem. Int. Ed.* **53**, 429–433 (2014).
25. Wang, G., Peng, Q. & Li, Y. Lanthanide-doped nanocrystals: synthesis, optical-magnetic properties, and applications. *Acc. Chem. Res.* **44**, 322–332 (2011).
26. Baati, T. *et al.* In depth analysis of the in vivo toxicity of nanoparticles of porous iron(III) metal-organic frameworks. *Chem. Sci.* **4**, 1597–1607 (2013).
27. Yang, Y. *et al.* In vitro and in vivo uncaging and bioluminescence imaging by using photocaged upconversion nanoparticles. *Angew. Chem. Int. Ed.* **51**, 3125–3129 (2012).
28. Bellido, E. *et al.* Understanding the colloidal stability of the mesoporous MIL-100(Fe) nanoparticles in physiological media. *Langmuir* **30**, 5911–5920 (2014).
29. Gao, F. *et al.* Doxorubicin loaded silica nanorattles actively seek tumors with improved anti-tumor effects. *Nanoscale* **4**, 3365–3372 (2012).
30. Hong, S. *et al.* The binding avidity of a nanoparticle-based multivalent targeted drug delivery platform. *Chem. Biol.* **14**, 107–115 (2007).
31. Chen, T. *et al.* One-step facile surface engineering of hydrophobic nanocrystals with designer molecular recognition. *J. Am. Chem. Soc.* **134**, 13164–13167 (2012).
32. Lu, G. *et al.* Imparting functionality to a metal–organic framework material by controlled nanoparticle encapsulation. *Nat. Chem.* **4**, 310–316 (2012).
33. Wei, Y., Lu, F., Zhang, X. & Chen, D. Synthesis of oil-dispersible hexagonal-phase and hexagonal-shaped NaYF4:Yb,Er nanoplates. *Chem. Mater.* **18**, 5733–5737 (2006).

Acknowledgments

This project is financially supported by the National Natural Science Foundation of China (NSFC 51202239, 51472233, 51332008, 51172228), and National Basic Research Program of China (2014CB643803).

Author contributions

Z.Y.H. and J.L. conceived the work and designed the experiments. K.R.D., Z.Y.H. and Y.X.Z. performed the experiments. X.J.L., C.X.L., X.R.D. and Z.Y.C. contributed to the analysis and interpretation of the experimental data. K.R.D. and Z.Y.H. wrote the paper. All authors participated in the scientific discussions and manuscript preparation.

Additional information

Supplementary information accompanies this paper at http://www.nature.com/scientificreports

Competing financial interests: The authors declare no competing financial interests.

How to cite this article: Deng, K. *et al.* Aptamer-Mediated Up-conversion Core/MOF Shell Nanocomposites for Targeted Drug Delivery and Cell Imaging. *Sci. Rep.* **5**, 7851; DOI:10.1038/srep07851 (2015).